Electric fields deduced from plasmapause motion in IMAGE EUV images

J. Goldstein,[1,2] R. A. Wolf,[1] B. R. Sandel,[3] and P. H. Reiff[1]

[1] The IMAGE extreme ultraviolet (EUV) imager obtained global images of the plasmasphere erosion of 10 July 2000, in which the nightside plasmapause moved inward by about $2\,R_E$ during 5–8 UT. We use plasmapause motion to infer the electric (E) field component tangent to the moving plasmapause; in general we lack knowledge of the perpendicular E-field component. In the midnight-to-dawn quadrant where the plasmapause shape is very nearly circular, the tangential E-field component is equal to the azimuthal electric field E_φ. Peak westward E-fields of 0.6–1.3 mV/m were found at the plasmapause between $L \approx 4-6$, an inner magnetospheric E-field that was 25% of the solar wind E-field. The MLT-concentration of the inferred E-field suggests that convective flows may produce partial indentation of the nightside plasmapause (especially in the midnight-to-dawn sector) that widens as the edges of the indentation propagate azimuthally.   INDEX TERMS: 2712 Magnetospheric Physics: Electric fields (2411); 2730 Magnetospheric Physics: Magnetosphere—inner; 2768 Magnetospheric Physics: Plasmasphere. Citation: Goldstein, J., R. A. Wolf, B. R. Sandel, and P. H. Reiff (2004), Electric fields deduced from plasmapause motion in IMAGE EUV images, Geophys. Res. Lett., 31, L01801, doi:10.1029/2003GL018797.

1. Introduction

[2] The traditional picture of the shrinkage of the plasmapause during an active period holds that the boundary simply $E \times B$-drifts in the time-varying large-scale convection electric (E) field; this view has been represented computationally by various authors (e.g., *Grebowsky* [1970] and *Spiro et al.* [1981]). It has also been suggested that instabilities or other more complicated processes might play an active role [*Carpenter and Lemaire*, 1997]. The extreme ultraviolet (EUV) imager on the IMAGE satellite [*Sandel et al.*, 2001] has provided previously unavailable global images of the plasmasphere with spatial and temporal resolutions of 0.1 R_E and 10 minutes. These global observations of plasmapause shape and dynamics may help determine whether the simple picture from the 1960s and 1970s is correct, or whether more subtle physics is involved. IMAGE EUV has already confirmed the existence of plasmaspheric drainage plumes, a prediction of the early models [*Grebowsky*, 1970; *Sandel et al.*, 2001].

[3] *Carpenter et al.* [1972] used the motion of whistler ducts during substorms to infer the equatorial distribution of the azimuthal component of the convection E-field. *Burch et al.* [2001] suggested a similar approach using EUV observations of the time-dependent plasmapause. *Goldstein et al.* [2003a] reported the first observation by IMAGE EUV of a nightside plasmaspheric erosion event on 10 July 2000, and other similar events have since been studied [*Spasojević et al.*, 2003; *Goldstein et al.*, 2003b, in press] In this letter we demonstrate that it is indeed possible to infer electric fields from plasmapause motion captured by EUV during erosion events. We apply our technique to the 10 July 2000 plasmasphere erosion.

2. EUV Plasmapause Extraction

[4] IMAGE EUV obtains global images of the plasmasphere by detecting 30.4-nm sunlight resonantly scattered by the He$^+$ ion population. In the EUV image of Figure 1a, the brightness of each pixel is proportional to the line-of-sight integrated He$^+$ column abundance (in cm^{-2}). The image has been mapped to the magnetic equator by assigning to each pixel the minimum dipole L-shell along its line of sight [*Roelof and Skinner*, 2000]. The plasmasphere is the green-white region surrounding the Earth out to radial distances of roughly $4-5\,R_E$ on the nightside. A slight drop in intensity behind the Earth is caused by the Earth's shadow ('S' in Figure 1a). The nightside plasmapause in 1(a) is identifiable as the sharp transition from green to speckled black color [*Goldstein et al.*, 2003c].

[5] We extracted plasmapause locations from thirty-three EUV snapshots between 4:03–9:30 UT on 10 July 2000. Figure 1 illustrates the plasmapause extraction technique using the 7:07 EUV image. Points along the plasmapause were manually selected (by clicking on an EUV image with a computer mouse) with an (average) azimuthal spacing of about 1 hour of magnetic local time (MLT). In Figure 1a these manually-selected ('click') points are overplotted on the EUV image as filled white circles. On much of the dayside no plasmapause was identifiable. For each EUV snapshot, an array of click points (r_j, φ_j) was obtained, where $r = LR_E$ and $\varphi = \pi(\mathrm{MLT} - 12)/12$.

[6] Each array of click points was interpolated by Fourier series expansion

$$R_{pp}(\varphi) = R_E \sum_{k=0}^{K} [C_k \cos(k\varphi) + S_k \sin(k\varphi)] \qquad (1)$$

where C_k and S_k are standard Fourier series coefficients except for the conventional zeroth terms which have been absorbed inside the summation in our expression. (Note $S_0 = 0$.) We limited the number of terms K in each

---
[1]Department of Physics and Astronomy, Rice University, Houston, Texas, USA.
[2]Now at Space Science and Engineering Division, Southwest Research Institute, San Antonio, Texas, USA.
[3]Lunar and Planetary Laboratory, University of Arizona, Tucson, Arizona, USA.
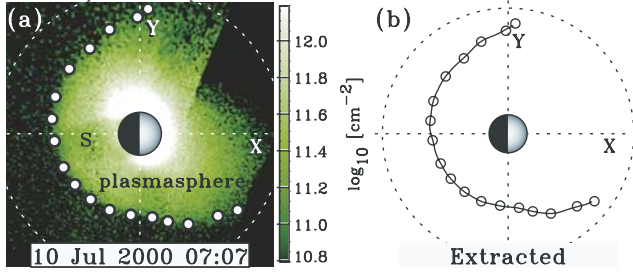
Figure 1. Example of extraction of plasmapause curve from IMAGE EUV, 10 July 2000, 7:07 UT. (a) EUV image, mapped to the magnetic equator (Earth at center; Sun to the right). Dotted lines are X- and Y-axes; dotted circle is geosynchronous orbit. The colorbar gives line-of-sight integrated He$^+$ column abundance. Black region in upper right is sunlight contamination. Filled white circles are manually-extracted ('click') points along the plasmapause. (b) Fourier expansion of the click points (circles) is plotted as the solid curve.

expansion according to the average azimuthal spacing $\Delta\varphi$ of each click point array: $K = \pi/\Delta\varphi$. K ranged from $10-15$ for the 33 Fourier expansions. In Figure 1b the click points (circles) and their Fourier expansion with $K = 13$ (solid curve) are plotted. The Fourier curve agrees with the 7:07 EUV plasmapause to within one or two pixels ($0.1-0.2$ R_E). Fourier interpolation allows each plasmapause curve to be represented analytically. The use of analytical expressions not only permits easy specification of the plasmapause radius at arbitrary φ, but also significantly simplifies the analysis (and reduces the computation) necessary to infer E-fields from the plasmapause motion. All of the time dependence of the 33 plasmapause curves of 10 July 2000 is contained in the Fourier coefficients C_k and S_k.

3. Electric Field From EUV Images

[7] The motion of the plasmapause boundary in a sequence of EUV images can be related to an equatorial electric field as follows. We assume that the boundary $R_{pp}(\varphi, t)$ is comprised of a large number cold plasma parcels subject only to $E \times B$ drift at the magnetic equator, and that these parcels will always collectively define the equatorial plasmapause, regardless of their motion. (Note: plasmapause $\neq$ Alfvén layer.) The $E \times B$ assumption includes the possibility of both contraction (i.e., compression) and erosion (i.e., removal) of the plasmapause plasma. In electric field $\mathbf{E} = E_r\hat{\mathbf{r}} + E_\varphi\hat{\varphi}$, cold plasma in magnetic field $\mathbf{B} = B\hat{\mathbf{r}} \times \hat{\varphi}$ will $E \times B$-drift both radially and azimuthally according to the equations of motion $\dot{r} = E_\varphi/B$ and $\dot{\varphi} = -E_r/(rB)$. If the detailed motions of the plasma parcels along the boundary $R_{pp}(\varphi, t)$ are known, then the vector E-field at that boundary is completely specified. The radial drift speed at the boundary is

$$\dot{r} = \dot{R}_{pp}(\varphi, t) = \left(\frac{\partial R_{pp}}{\partial \varphi}\right)_t \dot{\varphi} + \left(\frac{\partial R_{pp}}{\partial t}\right)_\varphi \quad (2)$$

where subscripts t or φ are held constant for partial derivatives. It is clear that $(\partial R_{pp}/\partial t)_\varphi \equiv V_{pp}$ is the radial speed of the plasmapause at a single MLT value, and $(\partial R_{pp}/\partial\varphi)_t$

describes the azimuthal variation of R_{pp} from a single EUV snapshot; both these quantities can be determined easily from (1) and arrays C_k and S_k. Inserting the equations of motion for $\dot{r}$ and $\dot{\varphi}$, and $V_{pp} = (\partial R_{pp}/\partial t)_\varphi$, into (2) gives

$$E_\varphi + \frac{E_r}{R_{pp}}\left(\frac{\partial R_{pp}}{\partial \varphi}\right)_t = V_{pp}B. \quad (3)$$

Defining the unit vector $\hat{\pi}$ tangent to the plasmapause R_{pp} as

$$\hat{\pi} = \left[\hat{\varphi} + \frac{1}{R_{pp}}\left(\frac{\partial R_{pp}}{\partial \varphi}\right)_t \hat{\mathbf{r}}\right]\cos\alpha \quad (4)$$

with

$$\cos\alpha \equiv \left[1 + \frac{1}{R_{pp}^2}\left(\frac{\partial R_{pp}}{\partial \varphi}\right)_t^2\right]^{-\frac{1}{2}} \quad (5)$$

allows (3) to be written

$$(\mathbf{E} \cdot \hat{\pi}) \equiv E_\pi = V_{pp} B \cos\alpha. \quad (6)$$

Thus a time-series of EUV-derived plasmapause curves does not provide a complete description of the electric field, but rather only the component (E_π) tangent to the moving plasmapause boundary. This is because it is difficult to estimate motion along the relatively smooth/featureless R_{pp} curves (such as plotted in Figure 1) that are typically observed by EUV on the nightside during erosions. Using (6) and assuming dipole B we determined the tangential E-field component E_π for the 33 EUV plasmapause curves between $4:03-9:30$ UT. The time derivatives of the Fourier coefficients C_k and S_k, required to obtain $V_{pp} = (\partial R_{pp}/\partial t)_\varphi$ from (1), were calculated by centered finite difference. The φ-derivatives were calculated analytically.

[8] As reported by *Goldstein et al.* [2003a], the 10 July erosion caused the nightside plasmapause to move about 2 R_E inward during $5-8$ UT. Most of the 10 July erosion was concentrated into two bursts of inward plasmapause motion during $5-6$ UT ('I') and $6:40-8$ UT ('II'). These bursts can be correlated with southward IMF transitions [*Goldstein et al.*, 2003a]. The most pronounced erosion in bursts (I) and (II) occurred at 5:25 and 7:07 UT respectively;
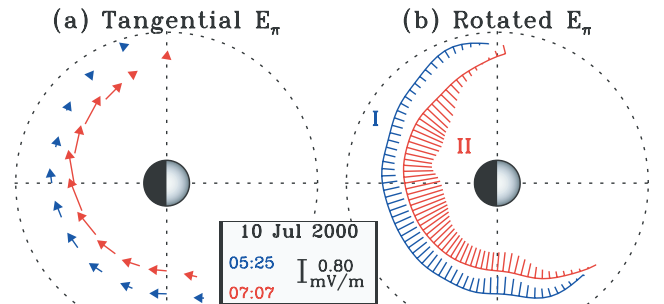

Figure 2. Equatorial plots showing EUV electric field tangential to the plasmapause at 5:25 UT (blue) and 7:07 UT (red) on 10 July 2000. (a) Tangential electric field vectors, scaled as 1 $R_E = 0.8$ mV/m. (b) Scaled flow-directions at plasmapause (E_π vectors rotated 90°).

(a) 10 Jul 2000 EUV Tangential E
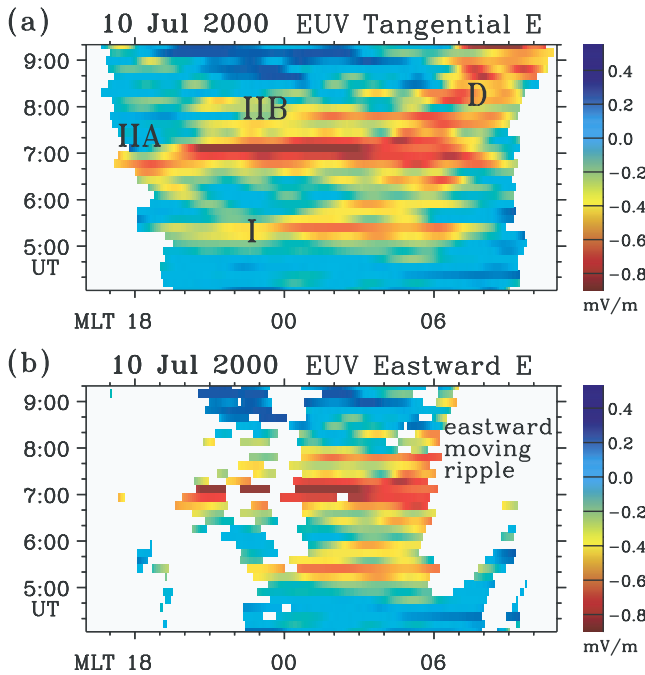

(b) 10 Jul 2000 EUV Eastward E

Figure 3. Electric field inferred from IMAGE EUV, 10 July 2000. (a) E_π (E-field tangent to the moving plasmapause boundary) versus UT and MLT. Colorbar gives strength in mV/m, saturated at -0.9 mV/m. (White = no data.) (b) E_φ (azimuthal E-field) estimated from E_π for cases in which $\alpha \leq 8°$, where $\cos \alpha \equiv (\hat{\pi} \cdot \hat{\varphi})$.

Figure 2 depicts our E_π determination at these two selected times. In 2(a) E_π vectors are drawn with their tails at the locations where they were obtained, and scaled as 1 $R_E = 0.8$ mV/m; vectors are only drawn at a few φ values to avoid cluttering up the plot. Another way to represent this data is shown in 2(b), which plots E_π vectors rotated 90° so that they point in the direction of the associated flows. We note that negative E_π points westward, and corresponds to radially inward plasmapause motion. From Figure 2, the peak E_π magnitude was about 1.3 mV/m and occurred during the second erosion burst (II). In burst (I), the peak $|E_\pi|$ (0.6 mV/m) was about half that of (II). From whistler duct motion, *Carpenter et al.* [1972] deduced westward E-fields of strength 0.5–0.6 mV/m, comparable to (I) but weaker than (II). We also note that our E-field strength is approximately 25% of the 10 July 2000 solar wind E-field reported by *Goldstein et al.* [2003a].

[9] Figure 3a shows inferred E_π values from the entire 10 July erosion event, plotted as intensity (color) versus UT and MLT. White (no color) means no E_π value was obtained (because no plasmapause was identifiable). The two main bursts (I) and (II) of erosion ($E_\pi < 0$) show up in 3(a) as horizontal bars of red/yellow (westward $|E_\pi| > 0.4$ mV/m). As mentioned above, E_π in burst (II) was stronger than burst (I). The MLT dependence of westward E_π will now be discussed, keeping in mind that 'westward' means $E_\pi < 0$. In (I), E_π is 1.3 to 1.5 times stronger within 0–7 MLT than at pre-midnight local times, and varies by only 10 percent within 0–7 MLT. Post-dawn E_π strength drops precipitously with increasing MLT, from

(6 MLT, -0.6 mV/m) to (8 MLT, -0.25 mV/m). Post-midnight concentration of westward E_π is consistent with the local-time dependence of penetration E-field noted by *Carpenter et al.* [1972] and seen in Jicamarca radar data [*Fejer and Scherliess*, 1995]. By 'penetration E-field' we mean the part of the convection E-field that penetrates the inner magnetospheric shielding layer [*Goldstein et al.*, 2003a]. The second burst (II) is separated into two intervals with different MLT dependences. In (IIA) E_π below -0.6 mV/m is found all across the nightside, between 20–07 MLT (varying by 30 percent within that MLT range), with the strongest westward E_π near midnight. As noted by *Goldstein et al.* [2003a], the second 10 July erosion burst (II) may have been intensified by a global magnetospheric compression that created a strong inductive E-field, which is consistent with the MLT dependence of (IIA). We note, however, that there was also a strong solar wind E-field (~5 mV/m) correlated with the second burst of erosion, so it is likely that both penetration and inductive E-fields contributed. Just before 8 UT, (IIB) shows similar MLT dependence to (I), so that (IIB) may also be interpreted as penetration E-field.

[10] From equation (4), $\cos \alpha \equiv (\hat{\pi} \cdot \hat{\varphi})$; i.e., if the plasmapause is perfectly circular, $\cos \alpha = 1$ and (6) reduces to $E_\varphi = V_{pp}B$, a purely azimuthal E-field. In general, however, E_π will contain contributions from both E_r and E_φ. To express E_π in terms of $\hat{r}$ and $\hat{\varphi}$ (more useful than the time-varying non-standard unit vector $\hat{\pi}$), we could: (A) estimate $\dot{\varphi}$ and use this estimate to compute E_r and E_φ from E_π; (B) apply the technique only for 'nearly circular' R_{pp} curves, thus obtaining an estimate for E_φ. In approach (A), $\dot{\varphi}$ could be estimated using modeling and/or additional measurements, but such (extensive) additional effort is beyond the scope of this letter, in which we seek merely to demonstrate what information can be extracted from EUV data alone. We therefore chose approach (B). In Figure 3b, E_π values for which $\alpha > 8°$ have been removed (set to white). The remaining data have $\alpha \leq 8°$, corresponding to $\cos \alpha \geq 0.99$. In other words, plotted in 3(b) is the subset of E_π data for which the plasmapause is very nearly circular; i.e., $(\hat{\pi} \cdot \hat{\varphi}) \approx 1$, and $E_\pi \approx E_\varphi$. In Figure 3b a good estimate for E_φ is thus obtained for the post-midnight (0–6 MLT) sector, and portions of pre-midnight at scattered times.

[11] We now discuss the regions of non-circularity, and what they imply for erosion dynamics. During the initial phase of the 10 July erosion, a broad plume of sunward-moving dayside plasma forms. As a result, the plasmapause is noncircular at the dawn and dusk flanks. Plasmapause non-circularity is also related to the MLT dependence of E_π discussed above. During the erosion, strong E_φ (i.e., strong radial flow) is concentrated in some MLT range ΔM (0–7 MLT for (I) and (IIB); 20–07 MLT for (IIA)) and is also roughly constant (to 10–30%) within ΔM. The plasmapause radius within ΔM is smaller than in surrounding areas and roughly circular, but at the edges of the sector ΔM the plasmapause bulges outward. These 'edge bulges' or 'ripples' then propagate azimuthally. Such an erosion scenario, involving partial indentation of the nightside plasmapause, was proposed by *Carpenter and Lemaire* [1997], and is supported by our results. In Figure 3a a broad diagonal band ('D') of red/yellow extends from
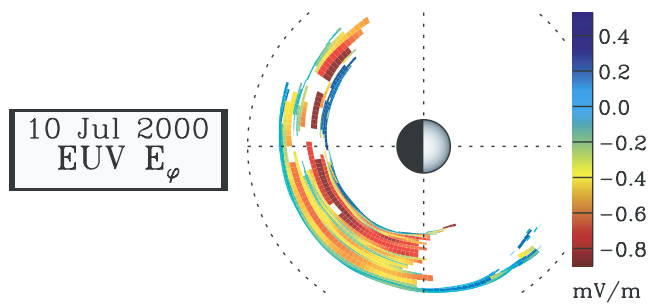
Figure 4. Azimuthal electric field component E_φ inferred from IMAGE EUV observations, 10 July 2000, plotted in the equatorial plane (Earth at center; Sun to right). The dotted circle is at geosynchronous orbit. Colorbar gives E_φ strength in mV/m.

(6 MLT, 7 UT) to (9 MLT, 9:20 UT); we attribute this to the formation of a dawnside bulge or ripple at the eastern edge of ΔM, that subsequently propagates eastward, creating the diagonal feature D. Note that in 3(b), which excludes non-circular plasmapause, the portion of the plot containing D is blocked out, indicating a ripple. From the slope of diagonal D the azimuthal flow speed is about 3 MLT-hours/2.3 UT-hours, or 1.3 times corotation. A similarly strong diagonal feature is not seen at the western edge of ΔM, perhaps because the azimuthal gradient in E_π is milder there than at the dawn terminator. In 3(b) there is a vertical band of non-circularity (white) close to midnight that may be associated with a plasmapause ripple, or may be an artifact of the Earth's shadow.

[12] IMAGE EUV observations can provide a uniquely global view of electric fields near the plasmapause. *Rowland and Wygant* [1998] used 10 months of CRRES data to produce a synoptic equatorial plot of the disturbance-time electric field. In Figure 4 we show a similar plot of E_φ, obtained from about 5 hours of EUV images during the 10 July disturbance. This plot is not precisely a synoptic plot in the same sense as that of *Rowland and Wygant* [1998] since it only shows E_φ along the moving plasmapause; to truly represent the average disturbance-time E-field would require more than one erosion event. However, for each erosion event the volume of data obtained by the global EUV imager is much greater than a satellite pass of in situ measurements, and E_φ along a given plasmapause curve is temporally correlated in a way not possible for single-point measurements in a given erosion event. From Figure 4 we see that westward E-field strengths above 0.4 mV/m were observed between $L \approx 4$ and $L \approx 6$.

4. Conclusions

[13] Recently there has been renewed interest in inner-magnetospheric and mid-latitude-ionospheric electric fields (e.g., *Rowland and Wygant* [1998]; *Burke et al.* [1998]; *Foster et al.* [2002]). We have demonstrated that E-fields may be inferred from global plasmapause motion observed by IMAGE EUV. We do not yet have a robust method of following the motion of individual plasma parcels along the plasmapause in EUV images. Therefore with no

additional information other than that provided by EUV we can infer only the component of electric field tangent to the plasmapause boundary. In the case that the plasmapause is roughly circular, the inferred tangential E-field component is approximately equal to the azimuthal electric field E_φ.

[14] Analysis of E_φ in particular events can shed light on some of the details of the erosion process. For the 10 July 2000 erosion event, we found peak westward E-field strengths of $0.6-1.3$ mV/m at plasmapauses between $L = 4$ and $L = 6$, an inner magnetospheric E-field magnitude that was 25% of the solar wind E-field. At some times during the erosion E_φ was concentrated mostly in post-midnight MLTs, consistent with a penetration E-field interpretation and with the results of *Carpenter et al.* [1972]; *Fejer and Scherliess* [1995] and *Carpenter and Lemaire* [1997]. During one interval, a larger MLT swath of the plasmapause moved inward at the same time, perhaps due to E-fields associated with a magnetospheric compression [*Goldstein et al.*, 2003a]. The erosion process may very well involve partial indentation of the nightside plasmapause in MLT sectors where E_φ is concentrated, as proposed by *Carpenter and Lemaire* [1997]. Bulges at the edges of the indentation propagate azimuthally, yielding a rough estimate of azimuthal flows. We have demonstrated how the technique of *Carpenter et al.* [1972] may be modified for use with EUV images to deduce E_φ information that is reasonable, but unvalidated by independent measurements. Validation is the next step in this project.

References

Burch, J. L., et al. (2001), Views of Earth's magnetosphere with the IMAGE satellite, *Science*, *291*, 619.

Burke, W., J. F. Rich, N. Maynard, M. Hagan, R. Wolf, G. Wilson, L. Gentile, M. Gussenhoven, C. Huang, and T. Garner (1998), Electrodynamics of the inner magnetosphere observed in the dusk sector by CRRES and DMSP during the magnetic storm of June 4–6, 1991, *J. Geophys. Res.*, *103*(A12), 29,399.

Carpenter, D. L., and J. Lemaire (1997), Erosion and recovery of the plasmasphere in the plasmapause region, *Space Sci. Rev.*, *80*, 153.

Carpenter, D. L., K. Stone, J. C. Siren, and T. L. Crystal (1972), Magnetospheric electric fields deduced from drifting whistler paths, *J. Geophys. Res.*, *77*, 2819.

Fejer, B., and L. Scherliess (1995), Time dependent response of equatorial ionospheric electric fields to magnetospheric disturbances, *Geophys. Res. Lett.*, *22*(7), 851.

Foster, J. C., P. J. Erickson, A. J. Coster, and J. Goldstein (2000), Ionospheric signatures of plasmaspheric tails, *Geophys. Res. Lett.*, *29*(13), 1623, doi:10.1029/2002GL015067.

Goldstein, J., B. R. Sandel, W. T. Forrester, and P. H. Reiff (2003a), IMF-driven plasmasphere erosion of 10 July 2000, *Geophys. Res. Lett.*, *30*(3), 1146, doi:10.1029/2002GL016478.

Goldstein, J., B. R. Sandel, and P. H. Reiff (2003b), Control of plasmaspheric dynamics by both convection and sub-auroral polarization stream, *Geophys. Res. Lett.*, in press.

Goldstein, J., M. Spasojević, P. H. Reiff, B. R. Sandel, W. T. Forrester, D. L. Gallagher, and B. W. Reinisch (2003c), Identifying the plasmapause in IMAGE EUV data using IMAGE RPI in situ steep density gradients, *J. Geophys. Res.*, *108*(A4), 1147, doi:10.1029/2002JA009475.

Grebowsky, J. M. (1970), Model study of plasmapause motion, *J. Geophys. Res.*, *75*, 4329.

Roelof, E. C., and A. J. Skinner (2000), Extraction of ion distributions from magnetospheric ENA and EUV images, *Space Sci. Rev.*, *91*, 437.

Rowland, D. E., and J. R. Wygant (1998), Dependence of the large-scale, inner magnetospheric electric field on geomagnetic activity, *J. Geophys. Res.*, *103*(A7), 14,959.

Sandel, B. R., R. A. King, W. T. Forrester, D. L. Gallagher, A. L. Broadfoot, and C. C. Curtis (2001), Initial results from the IMAGE extreme ultraviolet imager, *Geophys. Res. Lett.*, *28*(8), 1439.

Spasojević, M., J. Goldstein, D. L. Carpenter, U. S. Inan, B. R. Sandel, M. B. Moldwin, and B. W. Reinisch (2003), Global response of the plasmasphere to a geomagnetic disturbance, *J. Geophys. Res.*, *108*(A9), 1340, doi:10.1029/2003JA009987.

Spiro, R. W., M. Harel, R. A. Wolf, and P. H. Reiff (1981), Quantitative simulation of a magnetospheric substorm 3. Plasmaspheric electric fields and evolution of the plasmapause, *J. Geophys. Res.*, *86*, 2261.

———————————

J. Goldstein, Space Sci Div, Southwest Research Institute, San Antonio, TX 78228, USA. (jerru@alum.dartmouth.org)

R. A. Wolf and P. H. Reiff, Department of Physics and Astron, Rice University, Houston, TX 77005, USA.

B. R. Sandel, Lunar and Planetary Lab, University of Arizona, Tucson, AZ 85721, USA.